REPORT

www.the-innovation.org

Elevating thermoelectric performance in the sub-ambient temperature range for electronic refrigeration

Xiaojing Ma,[1,2,5] Chenhao Lin,[2,5] Hengyu Yang,[2,5] Yuhao Fu,[3] Kun Liang,[2] Xin Bao,[2] Sheng Ye,[2] Jian Wang,[4] Peng Zhao,[2] Jiang Chen,[2] Shizhen Zhi,[2] Longzhi Wu,[2] Sichen Duan,[2] Feng Cao,[4] Qian Zhang,[1,2,*] and Jun Mao[1,2,*]

*Correspondence: zhangqf@hit.edu.cn (Q.Z.); maojun@hit.edu.cn (J.M.)

Received: October 9, 2024; Accepted: February 27, 2025; Published Online: March 5, 2025; https://doi.org/10.1016/j.xinn.2025.100864

GRAPHICAL ABSTRACT

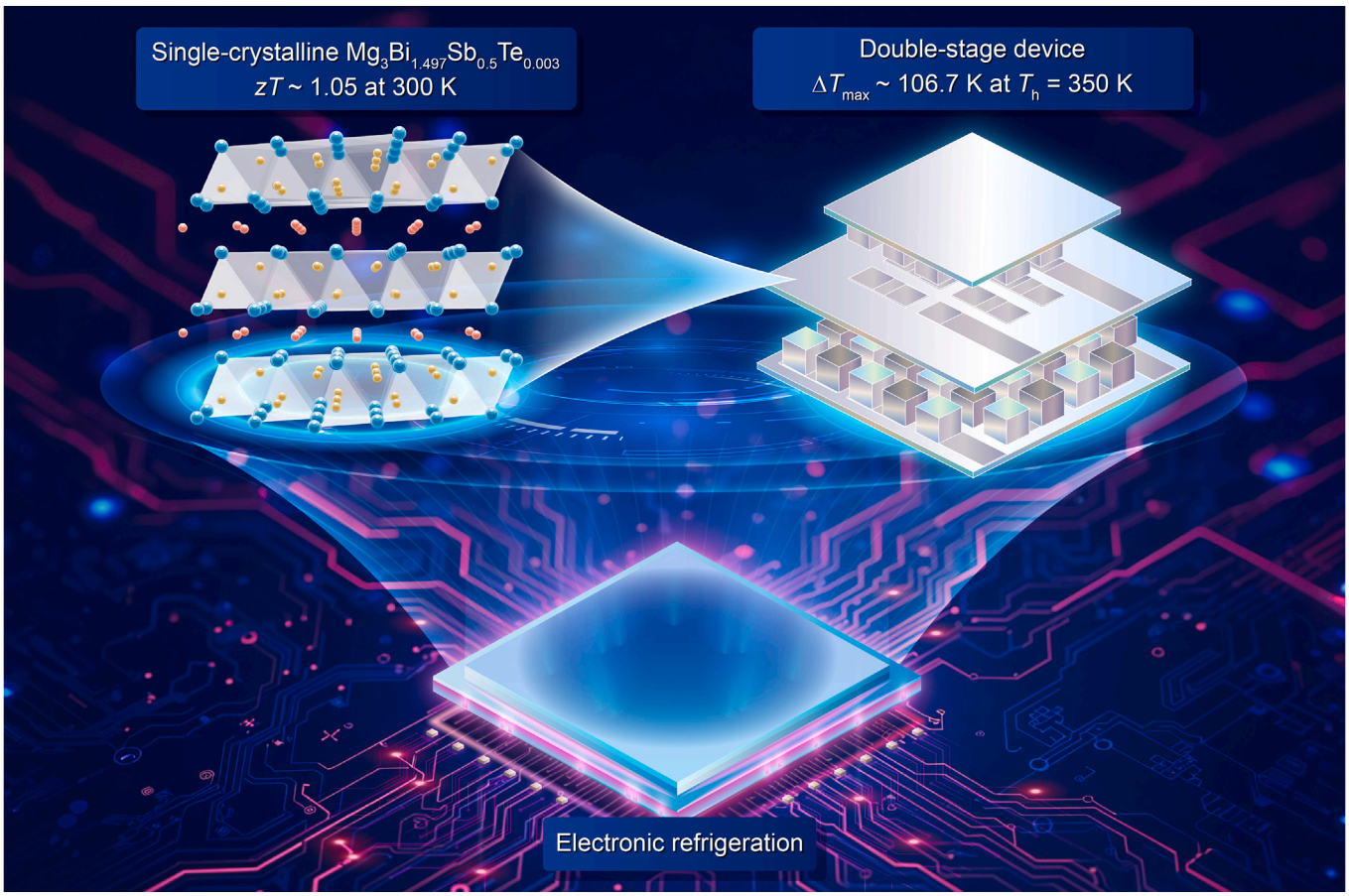

PUBLIC SUMMARY

- Centimeter-sized $Mg_3Bi_{2-x}Sb_x$ single crystals were synthesized by a slow-cooling method.
- Record-high thermoelectric performance was achieved in the sub-ambient temperature range.
- Double-stage cooler with a superior cooling performance of ~106.8 K exceeding commercial Bi_2Te_3 devices.
- More than 2,000 cycles of cooling performance measurements confirmed the superior stability of the cooler.
- The Mg_3Bi_2-based cooler is highly promising for applications in electronic thermal management.

OPEN ACCESS

REPORT

Elevating thermoelectric performance in the sub-ambient temperature range for electronic refrigeration

Xiaojing Ma,[1,2,5] Chenhao Lin,[2,5] Hengyu Yang,[2,5] Yuhao Fu,[3] Kun Liang,[2] Xin Bao,[2] Sheng Ye,[2] Jian Wang,[4] Peng Zhao,[2] Jiang Chen,[2] Shizhen Zhi,[2] Longzhi Wu,[2] Sichen Duan,[2] Feng Cao,[4] Qian Zhang,[1,2,*] and Jun Mao[1,2,*]

[1]State Key Laboratory of Precision Welding & Joining of Materials and Structures, Harbin Institute of Technology, Harbin 150001, China

[2]School of Materials Science and Engineering, and Institute of Materials Genome & Big Data, Harbin Institute of Technology (Shenzhen), Shenzhen 518055, China

[3]State Key Laboratory of Superhard Materials, College of Physics, Jilin University, Changchun 132000, China

[4]School of Science, Harbin Institute of Technology (Shenzhen), Shenzhen 518055, China

[5]These authors contributed equally

*Correspondence: zhangqf@hit.edu.cn (Q.Z.); maojun@hit.edu.cn (J.M.)

Received: October 9, 2024; Accepted: February 27, 2025; Published Online: March 5, 2025; https://doi.org/10.1016/j.xinn.2025.100864

Citation: Ma X., Lin C., Yang H., et al., (2025). Elevating thermoelectric performance in the sub-ambient temperature range for electronic refrigeration. The Innovation **6(5)**, 100864.

Solid-state thermoelectric coolers, which enable direct heat pumping by utilizing electricity, play an essential role in electronic refrigeration. Given that these devices usually cool down to the sub-ambient temperature range, their performance is critically dependent on the material properties at temperatures below 300 K. Consequently, enhancing the thermoelectric properties of materials at sub-ambient temperature is of paramount importance for advancing cooling technology. Herein, a single-crystalline Mg_3Bi_2-based material has been prepared and exhibits high electron mobility. As a result, thermoelectric figure-of-merit values of ∼1.05 at 300 K and ∼0.87 at 250 K (along the *ab* plane) have been achieved, which are superior to commercial n-type $Bi_2(Te, Se)_3$. Thermoelectric coolers (single- and double-stage devices) based on the n-type single-crystalline $Mg_3Bi_{1.497}Sb_{0.5}Te_{0.003}$ and p-type $(Bi, Sb)_2Te_3$ have been fabricated. The double-stage cooler demonstrates a remarkable maximum cooling temperature difference of ∼106.8 K at the hot-side temperature of 350 K, surpassing the performance of commercial Bi_2Te_3-based devices. Notably, the Mg_3Bi_2-based double-stage device exhibits exceptional cyclic stability, maintaining its cooling performance without any observable degradation after approximately 2,000 cycles between the input currents of 1 and 3 A. These findings show that single-crystalline Mg_3Bi_2 alloys hold great promise for thermoelectric cooling applications.

INTRODUCTION

Solid-state thermoelectric coolers can convert electricity into cooling and heating via the Peltier effect,[1–4] and they have been applied to electronic refrigeration and thermal management.[5,6] The cooling performance of the thermoelectric device, quantified by both the coefficient of performance (COP) and achievable temperature difference (ΔT), is fundamentally governed by the materials' dimensionless figure-of-merit (zT).[7–9] This critical parameter is defined as $zT = S^2T/(\kappa\rho)$, where S represents the Seebeck coefficient, κ denotes the thermal conductivity, ρ stands for the electrical resistivity, and T is the absolute temperature.

Since their discovery in the 1950s, Bi_2Te_3-based alloys have remained the cornerstone of commercial thermoelectric cooling technologies. Despite extensive research efforts in thermoelectric materials development, only a limited number of alternative compounds have demonstrated competitive performance near room temperature. These include MgAgSb,[10–12] SnSe,[13,14] Ag_2Se,[15–18] PbSe-based materials,[19,20] and the recently developed Mg_3Bi_2-based alloys,[21–30] which have emerged as promising candidates for thermoelectric cooling. Thermoelectric devices typically cool down to the sub-ambient temperature range (less than 250 K), making their performance critically dependent on material properties below 300 K.[31] Among the existing materials, Bi_2Te_3 alloys hold unparalleled zT values in this low-temperature range. The development of new materials exhibiting enhanced thermoelectric performance at sub-ambient temperatures presents both significant scientific challenges and technological implications for advancing efficient cooling solutions.

Herein, a single-crystalline $Mg_3Bi_{1.5}Sb_{0.5}$-based material has been prepared and optimized, and it exhibits zT values of ∼1.05 at 300 K and 0.87 at 250 K along the *ab* plane. These values surpass those of commercial n-type $Bi_2(Te, Se)_3$ alloys in the sub-ambient temperature range. By utilizing the n-type single-crystalline Mg_3Bi_2 alloys in conjunction with p-type $(Bi, Sb)_2Te_3$, both single- and double-stage thermoelectric coolers have been fabricated. A maximum cooling temperature difference of ∼106.8 K at the hot-side temperature of 350 K has been realized in the double-stage device, representing an improvement over the conventional Bi_2Te_3-based coolers.

MATERIALS AND METHODS

Crystal growth and material preparation

Mg_3Bi_2-based single crystals are prepared by using the slow cooling method. To prepare the Mg_3Bi_2-based single crystals, magnesium (Mg ingots, ZNXC, 99.995%), bismuth (Bi shots, ZNXC, 99.999%), antimony (Sb shots, ZNXC, 99.999%), and tellurium (Te ingots, ZNXC, 99.999%) were weighed according to the nominal composition of $Mg_{3.05}Bi_{1.997-x}Sb_xTe_{0.003}$ and $Mg_{3.05}Bi_{1.5-y}Sb_{0.5}Te_y$. The raw materials were sealed in the niobium tube (with an inner diameter of 22 mm and a length of 100 mm) with the partial pressure of argon using an arc welder. The niobium tubes were then sealed in the quartz tube in a vacuum. The sample was heated up to 1,223 K in 12 h, maintained at this temperature for 48 h, and then slowly cooled down to 923 K at the rate of 3 K h^{-1}, followed by annealing at this temperature for 72 h and then cooling down to room temperature.

Device fabrication

Single-crystalline $Mg_3Bi_{1.497}Sb_{0.5}Te_{0.003}$ was prepared into a disk with a diameter of ∼12.7 mm along the *ab* direction (in the device, the electric current will be applied parallel to the *c* direction of the crystal) and a thickness of ∼2.52 mm by wire cut electrical discharge machining. The raw elements of magnesium (Mg ingots, ZNXC, 99.995%) and nickel (Ni powder, ZNXC, 99.99%) were weighed according to the composition of Mg_2Ni in the glove box. These elements were sealed in the Nb tube and then encapsulated in the quartz tube. It was heated up to 1,223 K in 3 h, maintained at this temperature for 24 h, and then quenched in water. The ingot of the as-prepared Mg_2Ni was ball milled into powders. The junction of the Ag/Mg_2Ni/$Mg_3Bi_{1.497}Sb_{0.5}Te_{0.003}$/$Mg_2Ni$/Ag disk was prepared by spark plasma sintering of the Ag powder/Mg_2Ni powder/$Mg_3Bi_{1.497}Sb_{0.5}Te_{0.003}$ disk/Mg_2Ni powder/Ag powder together at a temperature of 623 K. The temperature increased from 300 to 623 K with a heating rate of 50 K min^{-1} and was maintained at 623 K temperature for 5 min under a compressive force of 3.5 kN. After that, the furnace was cooled down to room temperature. The sintering process for layered $Mg_3Bi_{1.497}Sb_{0.5}Te_{0.003}$ crystals impose dual constraints: high temperature can cause Mg evaporation, reducing carrier concentration which ultimately degrading the thermoelectric property. High sintering pressure will induce plastic deformation and weakening mechanical strength.

The sintered pellets were cut into legs by wire cutting (with the protection of oil) in a dimension of ∼1.9 × ∼1.9 × ∼3.2 mm. The contact layer of the p-type $(Bi, Sb)_2Te_3$ leg (RusTec) is electroplated in a $Ni(SO_3NH_2)_2$ solution after acid etching by HNO_3 (65%–68%). The p-type Ni/$(Bi, Sb)_2Te_3$/Ni junction was cut into the required dimension according to the simulation (Figure S1) by sand-wheel slice cutting in water. The optimal area ratio of A_n/A_p should be around 0.9 (1.71:1.9 mm). However, due to the wire-cutting accuracy and fabrication difficulties, the actual ratio of A_n/A_p for both the single- and double-stage modules is close to 1:1 (1.9:1.9 mm). The contact resistance of the thermoelectric leg is characterized by the homemade four-probe setup, and the contact resistance of the Ni/$(Bi, Sb)_2Te_3$/Ni is shown in Figure S2. The n- and p-type thermoelectric legs were soldered ($Sn_{42}Bi_{58}$, melting point: 411 K) to the ceramic plate deposited with Cu and Ni metals by a one-step reflow method performed with a reflow oven (T-937, Puhui). First, the temperature was raised to 408 K at a heating rate of 1 K s^{-1}, and the temperature was maintained at 393 K for 2 min. Then, the temperature was raised to 453 K at a heating rate of 1 K s^{-1}, and the temperature was kept at 453 K for 45 s. Finally, it was cooled to room temperature at a cooling rate of 1 K s^{-1}. The single- and double-stage devices based on commercial

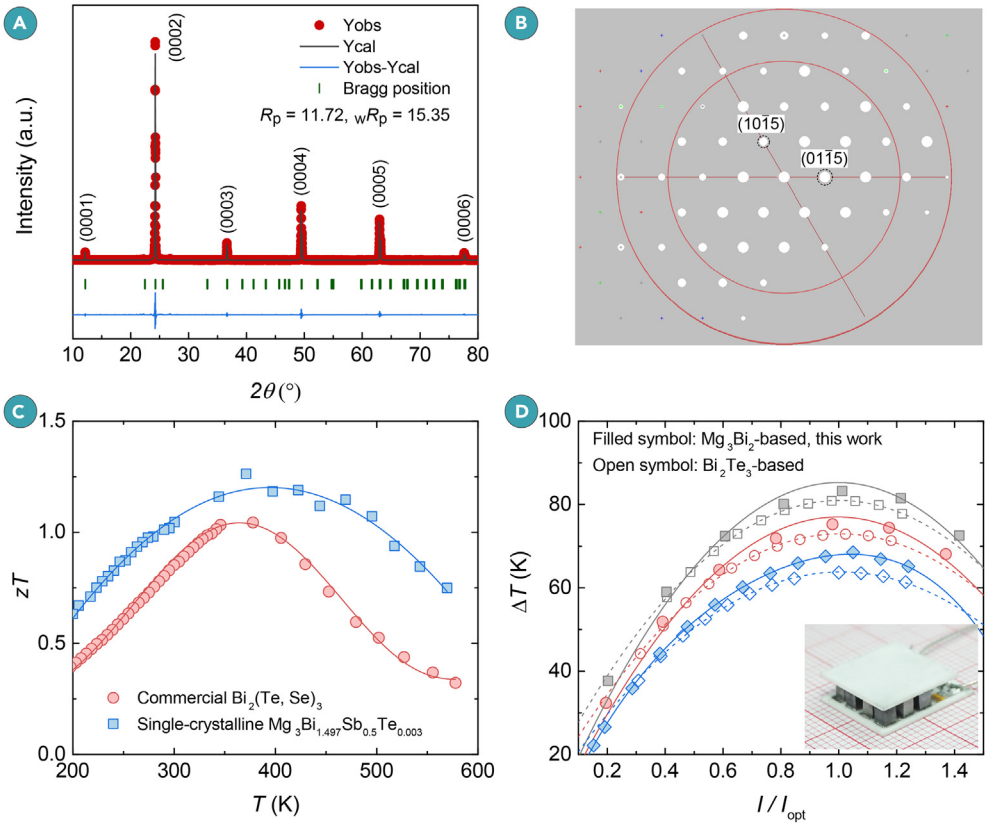

Figure 1. $Mg_3Bi_{1.497}Sb_{0.5}Te_{0.003}$ single crystal and the thermoelectric cooling performance of the device (A) X-ray diffraction and Rietveld refinement of single-crystalline $Mg_3Bi_{1.497}Sb_{0.5}Te_{0.003}$. (B) Single-crystal X-ray diffraction pattern of $Mg_3Bi_{1.497}Sb_{0.5}Te_{0.003}$ along the [0001] direction. (C) Comparison of the temperature-dependent zT between $Mg_3Bi_{1.497}Sb_{0.5}Te_{0.003}$ single crystal and commercial n-type $Bi_2(Te, Se)_3$. (D) Comparison of the cooling temperature difference between the single-crystalline $Mg_3Bi_{1.497}Sb_{0.5}Te_{0.003}$-based single-stage device and the device based on the commercial Bi_2Te_3 alloys. The blue, red, and gray symbols represent the results obtained at hot-side temperatures of 303, 325, and 350 K, respectively. The solid and dashed lines in (D) are the parabolic fitting of the measured data.

p-type $(Bi, Sb)_2Te_3$ (RusTec) and n-type $Bi_2(Te, Se)_3$ (RusTec) were fabricated by a similar process to that mentioned above.

RESULTS AND DISCUSSION

Growth of Mg_3Bi_2-based single crystals

The previously reported $Mg_3(Sb, Bi)_2$ crystals were primarily prepared by the Bridgman[32–35] and metal flux methods.[29,36–38] Layered $Mg_3(Sb, Bi)_2$ tends to crystallize into plate-like crystals with relatively small sizes when the metal flux method is used, which limits the fabrication of thermoelectric devices. In addition, the Bridgman method requires sophisticated equipment.[39] Herein, single-crystalline Mg_3Bi_2-based materials (with a nominal composition of $Mg_{3.05}Bi_{1.997-x}Sb_xTe_{0.003}$ and $Mg_{3.05}Bi_{1.5-y}Sb_{0.5}Te_y$) were prepared by the slow cooling method.[40] The obtained crystal can be easily cleaved along the (0001) plane (i.e., the *ab* plane), and the phase identification and crystal orientation are confirmed by X-ray diffraction (Figure 1A) and Laue diffraction (Figure S3). The crystallographic information of single-crystalline $Mg_3Bi_{1.497}Sb_{0.5}Te_{0.003}$ is collected by single-crystal X-ray diffraction, and the crystallographic data are shown in Tables S1–S4. The titled compound crystallized in the anti-La_2O_3 structure type in the trigonal space group $P\bar{3}m1$ (164), which features a cationic Mg1 sheet and an edge-shared $[MgBi_4]$ anionic tetrahedral layer.[36] The layered structure of the cleaved Mg_3Bi_2-based single crystal can be easily observed by scanning electron microscopy (SEM) (Figure S4A), and uniform elemental distribution is confirmed by energy-dispersive spectroscopy (EDS) (Figure S4B–S4E). The actual composition of the single crystal is determined to be $Mg_{3.04}Bi_{1.5}Sb_{0.5}$, while the Te content cannot be accurately quantified due to its low concentration. Figure 1C shows the comparison of the temperature-dependent zT between single-crystalline $Mg_3Bi_{1.497}Sb_{0.5}Te_{0.003}$ (along the *ab* plane) and commercial n-type $Bi_2(Te, Se)_3$ (Figure S5). The zT values of the $Mg_3Bi_{1.497}Sb_{0.5}Te_{0.003}$ single crystal reach ~1.05 at 300 K and ~0.87 at 250 K, demonstrating superior performance compared to n-type $Bi_2(Te, Se)_3$. Notably, the performance disparity between single-crystalline $Mg_3Bi_{1.497}Sb_{0.5}Te_{0.003}$ and $Bi_2(Te, Se)_3$ alloys becomes increasingly pronounced above the temperature of 350 K, primarily due to the more significant bipolar conduction in $Bi_2(Te, Se)_3$.

Benefitting from the superior thermoelectric performance, single-crystalline $Mg_3Bi_{1.497}Sb_{0.5}Te_{0.003}$ demonstrates exceptional potential for cooling applications. A single-stage thermoelectric device, comprising seven pairs of the n-type single-crystalline $Mg_3Bi_{1.497}Sb_{0.5}Te_{0.003}$ and p-type $(Bi, Sb)_2Te_3$, has been fabricated (the inset in Figure 1D). The experimentally determined maximum cooling temperature differences are approximately 69, 77, and 85 K at hot-side temperatures of 303, 325, and 350 K, respectively (Figure S6). This Mg_3Bi_2-based single-stage cooler outperforms the conventional device utilizing commercial n-type and p-type Bi_2Te_3 alloys (Figure 1D), showing lower cooling temperature differences of approximately 64, 73, and 81 K under identical hot-side temperatures (303, 325, and 350 K, respectively). A further comparison of the thermoelectric cooling performance has been conducted between the single-crystalline $Mg_3Bi_{1.497}Sb_{0.5}Te_{0.003}$-based single-stage device and various state-of-the-art polycrystalline devices, including Mg_3Bi_2-based materials,[23,41] MgAgSb,[42,43] SnSe,[14] and Bi_2Te_3 alloys[44–46] (Figure S7; Table S5). The experimental results demonstrate that the single-crystalline $Mg_3Bi_{1.497}Sb_{0.5}Te_{0.003}$-based device exhibits superior cooling performance to these reported thermoelectric coolers. In addition, commercial Bi_2Te_3-based single-stage devices from KELK (KSMH023), Marlow (SP5162-01AC), and Laird (CP14-71-10-L1-RT) have been characterized. The cooling temperature differences are 70 K for the KELK cooler and 65 K for both the Marlow and Laird devices (Figure S8; Table S6) at a hot-side temperature of 300 K. In other words, the single-crystalline $Mg_3Bi_{1.497}Sb_{0.5}Te_{0.003}$-based coolers are comparable to the KELK device (KSMH023) and higher than the others.

Thermoelectric performance of single-crystalline Mg_3Bi_2-based materials

The thermoelectric properties of single-crystalline $Mg_3Bi_{1.997-x}Sb_xTe_{0.003}$ and $Mg_3Bi_{1.5-y}Sb_{0.5}Te_y$ have been characterized, as shown in Figures S9 and S10. The transport properties of the $Mg_3Bi_{1.497}Sb_{0.5}Te_{0.003}$ single crystal along different crystallographic planes are shown in Figure 2. The electrical resistivity of single-crystalline $Mg_3Bi_{1.497}Sb_{0.5}Te_{0.003}$ is ~9.2 μΩ m along the *c* plane and ~7.7 μΩ m along the *ab* plane at a temperature of 250 K (Figure 2A). The disparity in electrical resistivity is not appreciable, and it can be ascribed to the similar Hall electron mobilities along different crystallographic planes. As shown in Figure 2C, the Hall electron mobility is ~457 $cm^2 V^{-1} s^{-1}$ along the *ab* plane and ~321 $cm^2 V^{-1} s^{-1}$ along the *c* plane at a temperature of 250 K. By eliminating grain boundaries and minimizing the concentration of other defects in single crystals, carrier mobility can be effectively improved, thus enhancing the electronic properties. The Seebeck coefficient is nearly identical along the *ab* and *c* planes, which exhibits the typical feature of semiconductors (Figure 2B). As a result, the power factor (S^2/ρ) in the *ab* plane is similar to that of the *c* plane (Figure S11). The power factor of single-crystalline $Mg_3Bi_{1.497}Sb_{0.5}Te_{0.003}$ is ~38 μW $cm^{-1} K^{-2}$ along the *ab* plane and ~34 μW $cm^{-1} K^{-2}$ along the *c* plane at a temperature of 250 K. The thermoelectric properties of single-crystalline $Mg_3Bi_{1.5}Sb_{0.5}$ have also been calculated along different crystallographic planes, and they are comparable (Figure S12), indicating that the thermoelectric properties are nearly isotropic.[33,47] Theoretical calculations reveal that the conduction

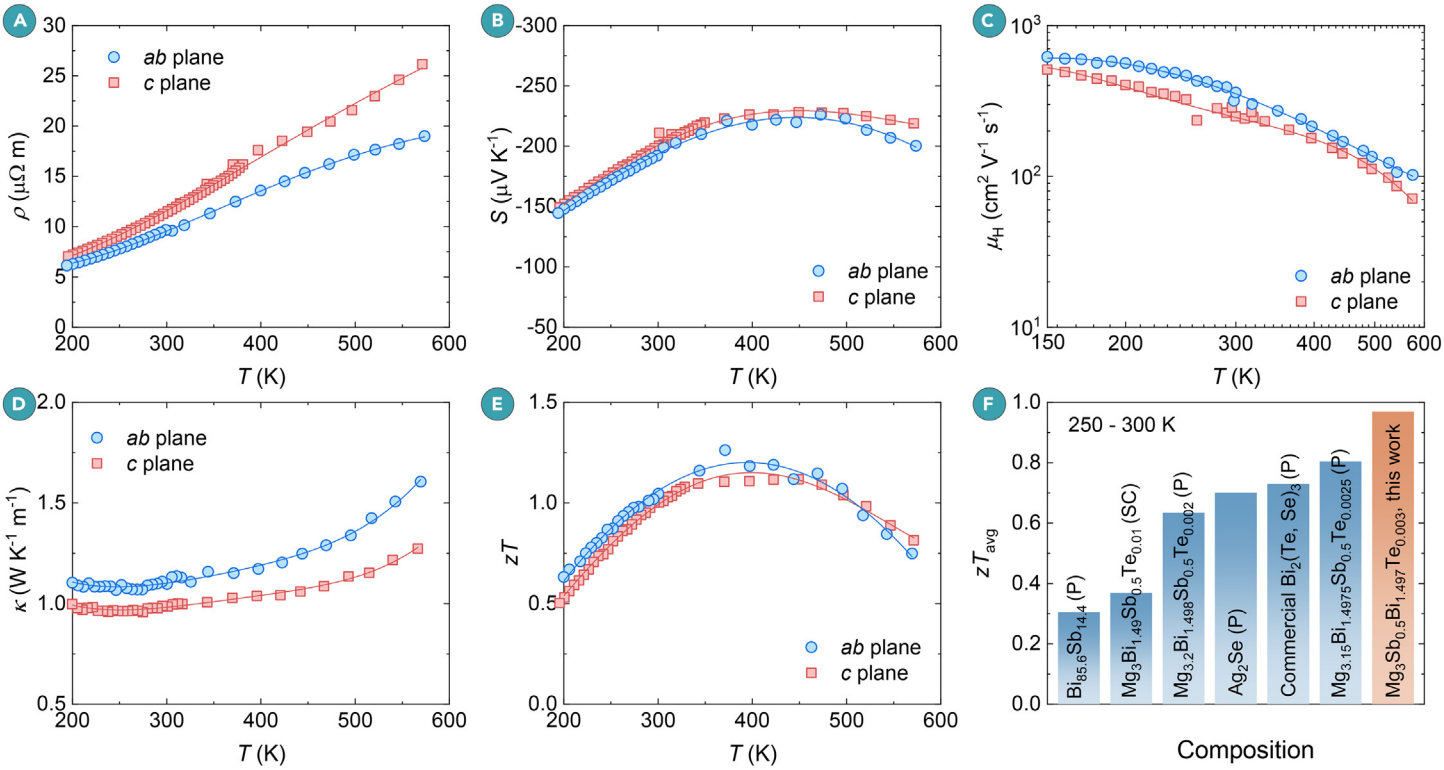

Figure 2. Thermoelectric properties of single-crystalline $Mg_3Bi_{1.497}Sb_{0.5}Te_{0.003}$ (A–E) Temperature-dependent (A) electrical resistivity, (B) Seebeck coefficient, (C) Hall electron mobility, (D) thermal conductivity, and (E) zT of $Mg_3Bi_{1.497}Sb_{0.5}Te_{0.003}$ along *ab* plane and *c* plane. (F) A comparison of the average zT in the temperature range between 250 and 300 K among different materials.[22,23,32,50,51] SC stands for the single-crystalline sample, and P stands for the polycrystalline sample.

band Fermi surface of $Mg_3Bi_{1.5}Sb_{0.5}$ shows weak anisotropy[48] (Figures S13 and S14), supported by the nearly isotropic conductivity effective masses. Specifically, the calculated conductivity effective masses of electrons is ~0.24 m_0 (where m_0 is the free electron mass) along the *ab* plane and ~0.21 m_0 along the *c* plane at a carrier concentration of 2×10^{19} cm^{-3}. The observed isotropic thermoelectric behavior in Mg_3Bi_2-based materials, while structurally layered, finds its origin in the three-dimensional charge transport characteristic enabled by the nearly isotropic interatomic bonding network.[49]

The measured thermal conductivity and zT of single-crystalline $Mg_3Bi_{1.497}Sb_{0.5}Te_{0.003}$ along different crystallographic planes are shown in Figure 2D. The thermal conductivity in the *ab* plane is slightly higher than that of the *c* plane, and the estimated sums of lattice thermal conductivity and bipolar thermal conductivity are also similar (Figure S15). As a result, the zTs are comparable along the *ab* plane and the *c* plane (Figure 2E). The thermal stability of single-crystalline $Mg_3Bi_{1.997-x}Sb_xTe_{0.003}$ has been evaluated through cyclic thermoelectric properties measurements across the temperature range of 300–573 K, encompassing five complete heating and cooling cycles. The measured thermoelectric properties are highly comparable (Figures S16–S18), which confirms the thermal stability of the material under operational conditions. Additionally, the reproducibility of the thermoelectric performance for single crystals from different batches has been verified and shows comparable results within the uncertainty of the measurements (Figures S19 and S20). A comparison of the average zT (zT_{avg}) in the temperature range between 250 and 300 K is presented in Figure 2F, encompassing various state-of-the-art materials, including polycrystalline Mg_3Bi_2-based materials,[22,23,32] Ag_2Se,[50] $Bi_{1-x}Sb_x$ alloys,[51] $Bi_2(Te, Se)_3$, and single-crystalline $Mg_3Bi_{1.497}Sb_{0.5}Te_{0.003}$. Single-crystalline $Mg_3Bi_{1.497}Sb_{0.5}Te_{0.003}$ exhibits a high average zT of ~0.97 along the *ab* plane, outperforming all other compared materials.

Fabrication of the single-crystalline Mg_3Bi_2-based double-stage device

To further evaluate the performance of single-crystalline $Mg_3Bi_{1.497}Sb_{0.5}Te_{0.003}$, single- (the inset of Figure 1D) and double-stage devices based on n-type $Mg_3Bi_{1.497}Sb_{0.5}Te_{0.003}$ and p-type $(Bi, Sb)_2Te_3$ have been fabricated. The double-stage device comprises a hierarchical arrangement of 7 thermoelectric pairs in the upper stage and 17 pairs in the lower stage (Figure 3D). The n-type thermoelectric legs feature a multilayer structure of $Ag/Mg_2Ni/Mg_3Bi_{1.497}Sb_{0.5}Te_{0.003}/Mg_2Ni/Ag$, fabricated by spark plasma sintering. In this configuration, Mg_2Ni serves as the contact layer, providing both low interfacial contact resistivity (ρ_c) and good mechanical bonding strength,[52] while Ag is chosen as the soldering layer. SEM combined with EDS (SEM-EDS) analysis of the interfaces reveals no observable secondary phase formation or elemental diffusion (Figure S21). The interfacial contact resistivity of the $Ag/Mg_2Ni/Mg_3Bi_{1.497}Sb_{0.5}Te_{0.003}/Mg_2Ni/Ag$ joint is ~2.1 $\mu\Omega$ cm^2 (Figure S22). The multilayer junction of $Ag/Mg_2Ni/Mg_3Bi_{1.497}Sb_{0.5}Te_{0.003}/Mg_2Ni/Ag$, integrated with Cu interconnects, was subjected to an isothermal aging process at 360 K (10 K higher than the maximum service temperature of 350 K) for 14 days. Post-aging characterization through contact resistance measurement and combined SEM-EDS analysis show preserved interfacial integrity with low contact resistivity and sharp phase boundaries (Figures S23–S25), indicating the reliability of the joints.

The prepared $Ag/Mg_2Ni/Mg_3Bi_{1.497}Sb_{0.5}Te_{0.003}/Mg_2Ni/Ag$ disks are sectioned into legs using wire cutting with oil protection (Figure 3A). Comparative characterization of single-crystalline $Mg_3Bi_{1.497}Sb_{0.5}Te_{0.003}$ before and after the sintering process reveals similar thermoelectric properties (Figure S26). The thermoelectric performance of the p-type Bi_2Te_3-based alloys is characterized in the temperature range of 200–600 K (Figure S27). The p-type $Ni/(Bi, Sb)_2Te_3/Ni$ disk is prepared by Ni electroplating followed by sand-wheel slice cutting into legs (Figure 3A). The SnBi solder is uniformly applied to the top, middle, and bottom ceramic substrates using stencil printing (Figure 3B). Following this, the thermoelectric legs are precisely positioned and assembled onto the bottom and top substrates with the aid of a fixture (Figure 3C), and the double-stage device is then assembled step by step using a custom-made fixture (Figure 3D). Finally, the fully assembled device is subjected to a one-step reflow soldering process for integration, and the fabricated double-stage cooler is shown in Figure 3.

Cooling performance of single-crystalline Mg_3Bi_2-based device

The cooling performance of the $Mg_3Bi_{1.497}Sb_{0.5}Te_{0.003}/(Bi, Sb)_2Te_3$ double-stage device is characterized by a homemade apparatus, as illustrated in Figure 4A. Two T-type thermocouples are securely fixed on the hot and cold sides of the double-stage device to monitor the hot-side temperature (T_h) and cold-side temperature (T_c) in real time. This setup enables the direct measurement

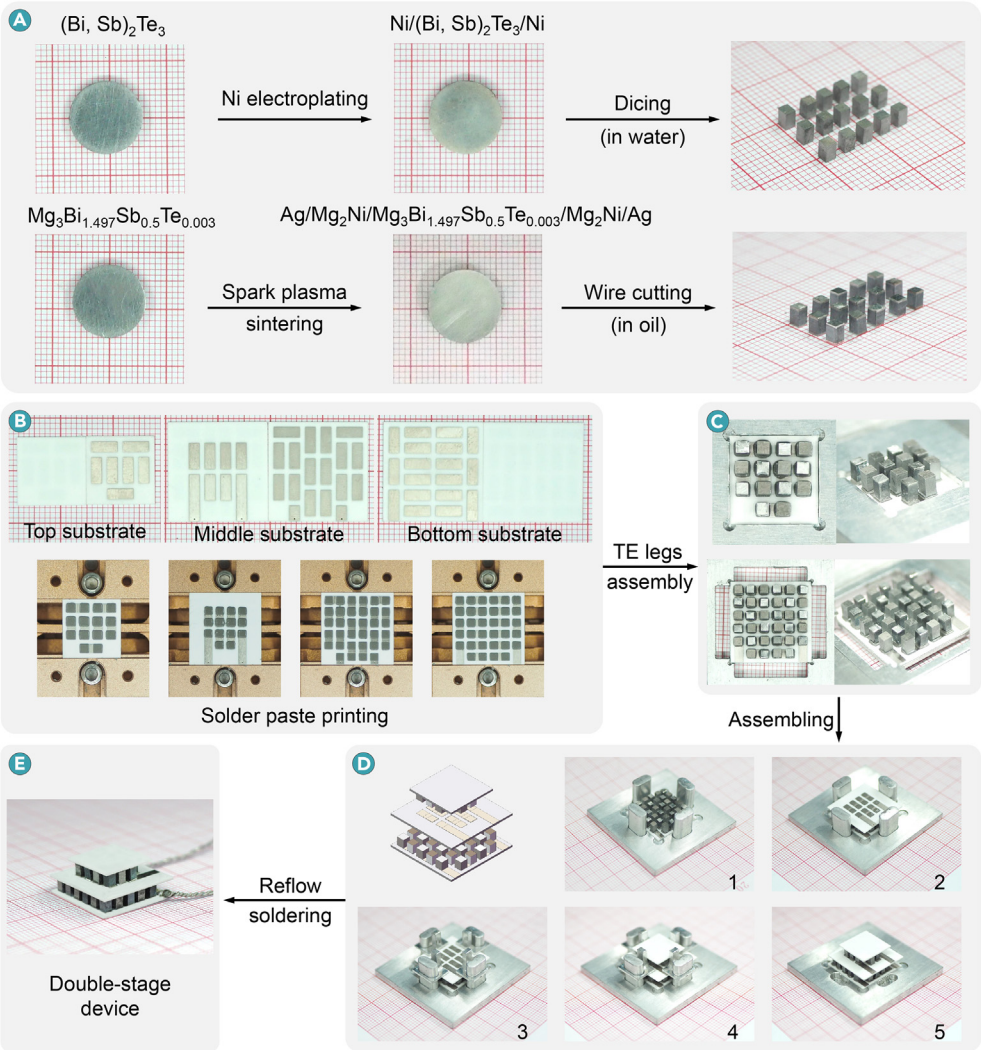

Figure 3. The fabrication of the single-crystalline $Mg_3Bi_{1.497}Sb_{0.5}Te_{0.003}$/(Bi, Sb)$_2Te_3$ double-stage device (A) Contact layer bonding and dicing. (B) Solder paste printing. (C) Leg assembly for each stage. (D) Device assembly. (E) The fabricated double-stage device after reflow soldering.

of the cooling temperature difference ($\Delta T = T_h - T_c$) once the system reaches a steady state. Based on the linear relationship between cooling temperature difference and cooling power, the cooling temperature differences at zero cooling power are extrapolated for each applied input electric current. By fitting a parabolic curve to the measured temperature differences as a function of input electric current, the maximum cooling temperature difference (ΔT_{max}) at a given hot-side temperature is determined. In addition, four T-type thermocouples (with readings T_1, T_2, T_3, and T_4) are evenly fixed along the centerline of the standard sample to measure the heat load applied to the cold side of the device. It should be noted that the measured heat flow corresponds to the cooling power (Q_c) of the double-stage device. Using these data, the COP is evaluated as the ratio of cooling power to the input electrical power, providing another critical metric to evaluate the cooler's performance.[53]

The relationship between the cooling power and the temperature difference of the double-stage module at different hot-side temperatures is shown in Figures 4B, S28, and S29. The cooling power exhibits a linear decrease as the cooling temperature difference increases. Consequently, the cooling power reaches its maximum value when the temperature difference is zero for a given input electric current.[8,9] The uncertainty analysis of the measured heat flow has been discussed in the supplemental information, and the results are shown in Figures S30 and S31. The relationship between the cooling power and input electric current is shown in Figure 4C. By parabolic fitting of the cooling power as a function of input electric current, the maximum cooling power is determined to be ~2.7 W, achieved at an optimal electric current (I_{opt}) of ~3.5 A. The COP also shows a good linear relationship with temperature difference in Figure 4D, and the relationship between COP and electric current is further shown in Figure 4E.

The input-electrical-current-dependent cooling temperature differences are shown in Figure 4F, and the maximum cooling temperature differences of this double-stage device are ~83.1, ~94.5, and ~106.8 K at hot-side temperatures of 303, 325, and 350 K, respectively (Figure 4F). The simulated cooling temperature differences (represented by dashed lines in Figure 4F) are slightly higher than the experimentally measured data, which can be ascribed to the non-vanishing electrical contact resistance. The stability of this double-stage device is evaluated by the cyclic measurement of cooling performance between the electrical currents of 1 and 3 A, as illustrated in Figure 4G. The device demonstrates superior stability, with cooling temperature differences maintaining consistency even after undergoing 2,000 continuous cycles (exceeding 320 h of operation). In addition, a double-stage device consisting of commercial p-type (Bi, Sb)$_2$Te$_3$ and n-type Bi$_2$(Te, Se)$_3$ has also been fabricated, and the maximum cooling temperature differences are ~79, ~94, and ~103 K at hot-side temperatures of 303, 325, and 350 K, respectively (Figure S32). In other words, the $Mg_3Bi_{1.497}Sb_{0.5}Te_{0.003}$/(Bi, Sb)$_2Te_3$ double-stage cooler exhibits superior cooling performance compared with the one based on commercial n-type/p-type Bi$_2$Te$_3$ alloys.

CONCLUSION

To sum up, single-crystalline $Mg_3Bi_{1.497}Sb_{0.5}Te_{0.003}$ has been prepared, and the thermoelectric transport properties along different crystallographic planes have been investigated. The $Mg_3Bi_{1.497}Sb_{0.5}Te_{0.003}$ single crystal exhibits a zT value exceeding 1.0 at 300 K and maintaining ~0.87 at 250 K, outperforming commercial n-type Bi$_2$(Te, Se)$_3$ alloys. Importantly, single- and double-stage thermoelectric coolers utilizing n-type single-crystalline $Mg_3Bi_{1.497}Sb_{0.5}Te_{0.003}$ and p-type (Bi, Sb)$_2$Te$_3$ have been fabricated. The double-stage device demonstrates a maximum temperature difference of ~106.8 K at a hot-side temperature of 350 K, which outperforms the cooler based on commercial n-type/p-type Bi$_2$Te$_3$ alloys. Our findings show that single-crystalline Mg$_3$Bi$_2$-based materials are highly promising for thermoelectric cooling applications.

DATA AND CODE AVAILABILITY

All data needed to evaluate the conclusions in the paper are present in the paper and/or the supplemental information.

REFERENCES

1. DiSalvo, F. (1999). Thermoelectric cooling and power generation. *Science* **285**:703–706.
2. Bell, L.E. (2008). Cooling heating generating power and recovering waste heat with thermoelectric systems. *Science* **321**:1457–1461.
3. He, J. and Tritt, T.M. (2017). Advances in thermoelectric materials research: Looking back and moving forward. *Science* **357**:eaak9997. DOI:https://doi.org/10.1126/science.aak9997.
4. Mao, J., Chen, G. and Ren, Z. (2021). Thermoelectric cooling materials. *Nat. Mater.* **20**:454–461.
5. Anatychuk, L. (1995). In CRC Handbook of Thermoelectrics, D.M. Rowe, ed. (CRC Press), p. 454. Ch. 50. https://doi.org/10.1201/9781420049718.
6. Semenyuk, V.A., Pilipenko, T.V., Albright, G.C. et al. (1994). Miniature thermoelectric coolers for semiconductor lasers. *AIP Conf. Proc.* **316**:150–153.
7. Ioffe, A.F., Stil'bans, L.S., Iordanishvili, E.K. et al. (1959). Semiconductor thermoelements and thermoelectric cooling. Infosearch. *Phys. Today* **12**:42.
8. Goldsmid, H. (1986). Electronic Refrigeration (Pion), p. 454. DOI:https://doi.org/10.1007/978-1-4899-5723-8-6.

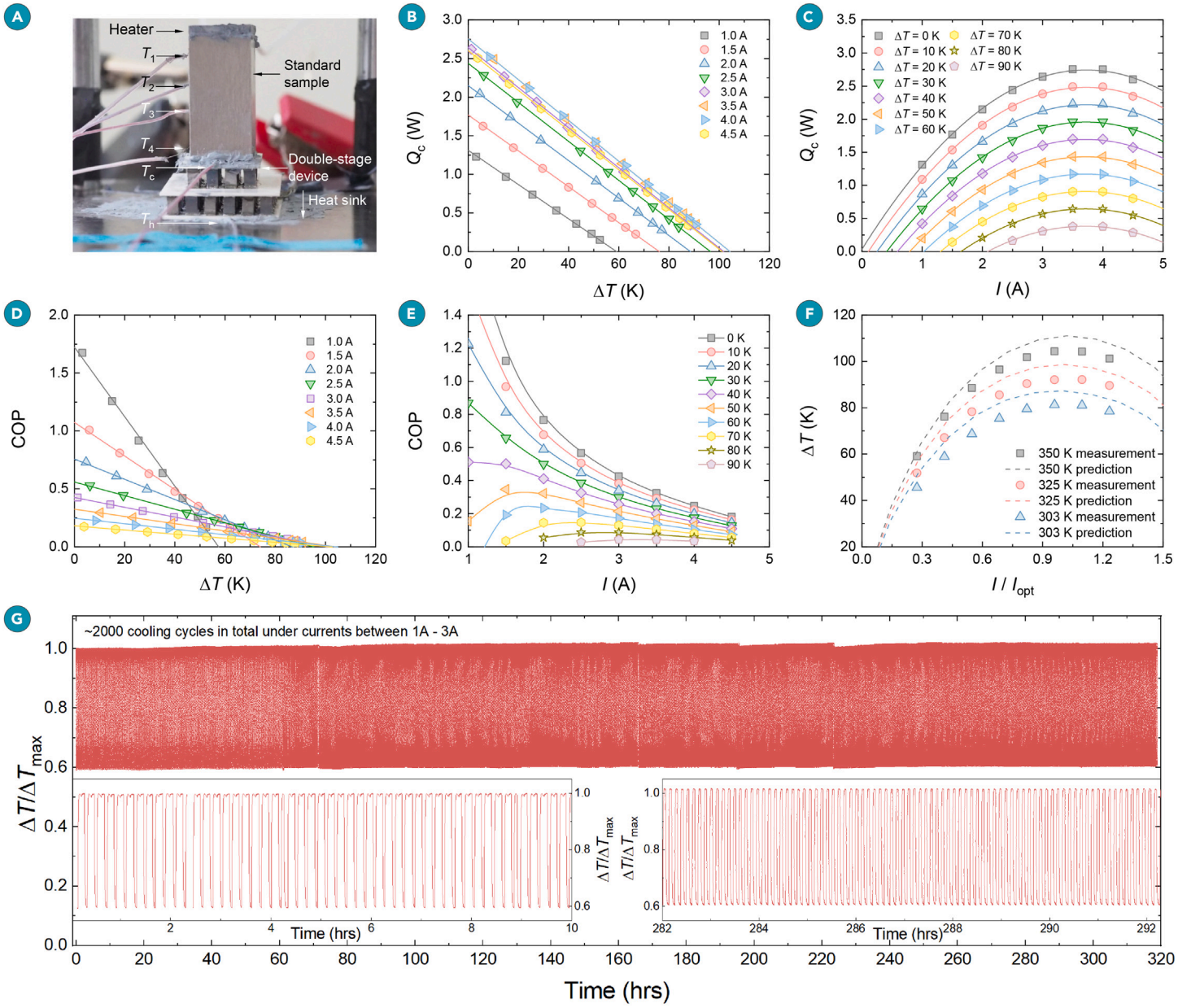

Figure 4. Thermoelectric cooling performance of the $Mg_3Bi_{1.497}Sb_{0.5}Te_{0.003}$/(Bi, Sb)$_2Te_3$ double-stage device (A) Setup for characterizing the cooling performance of the $Mg_3Bi_{1.497}Sb_{0.5}Te_{0.003}$/(Bi, Sb)$_2Te_3$ double-stage device. (B) Relationship between cooling power and temperature difference at a hot-side temperature of 350 K. (C) Relationship between cooling power and electric current at a hot-side temperature of 350 K. (D) Relationship between COP and temperature difference at a hot-side temperature of 350 K. (E) Relationship between COP and electric current at a hot-side temperature of 350 K. (F) Relationship between temperature difference and normalized electric current of the double-stage device at hot-side temperatures of 303, 325, and 350 K, respectively. (G) Cycling cooling performance for approximately 2,000 cycles (over 320 h) between electrical currents of 1 and 3 A.

9. Goldsmid, H. (1964). Thermoelectric Refrigeration (Springer US), p. 454. DOI:https://doi.org/10.1007/978-1-4899-5723-8.
10. Zhao, H., Sui, J., Tang, Z. et al. (2014). High thermoelectric performance of MgAgSb-based materials. *Nano Energy* **7**:97–103.
11. Liu, Z., Wang, Y., Mao, J. et al. (2016). Lithium doping to enhance thermoelectric performance of MgAgSb with weak electron-phonon coupling. *Adv. Energy Mater.* **6**:1502269. DOI:https://doi.org/10.1002/aenm.201502269.
12. Liu, Z., Sato, N., Gao, W. et al. (2021). Demonstration of ultrahigh thermoelectric efficiency of ~7.3% in Mg_3Sb_2/MgAgSb module for low-temperature energy harvesting. *Joule* **5**:1196–1208.
13. Liu, D., Wang, D., Hong, T. et al. (2023). Lattice plainification advances highly effective SnSe crystalline thermoelectrics. *Science* **380**:841–846.
14. Qin, B., Wang, D., Liu, X. et al. (2021). Power generation and thermoelectric cooling enabled by momentum and energy multiband alignments. *Science* **373**:556–561.
15. Jiang, F., Lin, C., Cheng, J. et al. (2025). Prefer-oriented Ag_2Se crystal for high-performance thermoelectric cooling. *Adv. Funct. Mater.* **35**:2415000. DOI:https://doi.org/10.1002/adfm.202415000.
16. Conn, J.B. and Taylor, R.C. (1960). Thermoelectric and crystallographic properties of Ag_2Se. *J. Electrochem. Soc.* **107**:977–982.
17. Mi, W., Qiu, P., Zhang, T. et al. (2014). Thermoelectric transport of Se-rich Ag_2Se in normal phases and phase transitions. *Appl. Phys. Lett.* **104**:133903. DOI:https://doi.org/10.1063/1.4870509.
18. Day, T., Drymiotis, F., Zhang, T. et al. (2013). Evaluating the potential for high thermoelectric efficiency of silver selenide. *J. Mater. Chem. C* **1**:7568–7573.
19. Wang, S., Wen, Y., Zhu, Y. et al. (2024). High carrier mobility and promising thermoelectric module performance of n-type PbSe crystals. *Small* **20**:2400866. DOI:https://doi.org/10.1002/smll.202400866.
20. Wang, L., Wen, Y., Bai, S. et al. (2024). Realizing thermoelectric cooling and power generation in n-type $PbS_{0.6}Se_{0.4}$ via lattice plainification and interstitial doping. *Nat. Commun.* **15**:3782.
21. Imasato, K., Kang, S.D. and Snyder, G.J. (2019). Exceptional thermoelectric performance in $Mg_3Sb_{0.6}Bi_{1.4}$ for low-grade waste heat recovery. *Energy Environ. Sci.* **12**:965–971.
22. Mao, J., Zhu, H., Ding, Z. et al. (2019). High thermoelectric cooling performance of n-type Mg_3Bi_2-based materials. *Science* **365**:495–498.
23. Chen, N., Zhu, H., Li, G. et al. (2023). Improved figure of merit (z) at low temperatures for superior thermoelectric cooling in Mg_3(Bi, Sb)$_2$. *Nat. Commun.* **14**:4932.
24. Tamaki, H., Sato, H.K. and Kanno, T. (2016). Isotropic conduction network and defect chemistry in Mg_3Sb_2-based layered Zintl compounds with high thermoelectric performance. *Adv. Mater.* **28**:10182–10187.

25. Zhang, J., Song, L., Pedersen, S.H. et al. (2017). Discovery of high-performance low-cost n-type Mg_3Sb_2-based thermoelectric materials with multi-valley conduction bands. *Nat. Commun.* **8**:13901. DOI:https://doi.org/10.1038/ncomms13901.
26. Kanno, T., Tamaki, H., Sato, H.K. et al. (2018). Enhancement of average thermoelectric figure of merit by increasing the grain-size of $Mg_{3.2}Sb_{1.5}Bi_{0.49}Te_{0.01}$. *Appl. Phys. Lett.* **112**:033903. DOI:https://doi.org/10.1063/1.5016488.
27. Shi, X., Zhao, T., Zhang, X. et al. (2019). Extraordinary n-type Mg_3SbBi thermoelectrics enabled by yttrium doping. *Adv. Mater.* **31**:1903387. DOI:https://doi.org/10.1002/adma.201903387.
28. Shu, R., Zhou, Y., Wang, Q. et al. (2019). $Mg_3Sb_xBi_{2-x}$ family: a promising substitute for the state-of-the-art n-type thermoelectric materials near room temperature. *Adv. Funct. Mater.* **29**:1807235. DOI:https://doi.org/10.1002/adfm.201807235.
29. Pan, Y., Yao, M., Hong, X. et al. (2020). $Mg_3(Bi,Sb)_2$ single crystals towards high thermoelectric performance. *Energy Environ. Sci.* **13**:1717–1724.
30. Bano, S., Chetty, R., Babu, J. et al. (2024). $Mg_3(Sb,Bi)_2$-based materials and devices rivaling bismuth telluride for thermoelectric power generation and cooling. *Device* **2**:100408. DOI:https://doi.org/10.1016/j.device.2024.100408.
31. Zhang, S., Liu, Z., Zhang, X. et al. (2024). Sustainable thermal energy harvest for generating electricity. *Innovation* **5**(2):100591. DOI:https://doi.org/10.1016/j.xinn.2024.100591.
32. Wang, Q., Li, F., Xia, S. et al. (2022). In-Situ loading bridgman growth of $Mg_3Bi_{1.49}Sb_{0.5}Te_{0.01}$ bulk crystals for thermoelectric applications. *Adv. Electron. Mater.* **8**(4):2101125. DOI:https://doi.org/10.1002/aelm.202101125.
33. Wang, Q.Q., Liu, K.F., Su, Y.Y. et al. (2023). High thermoelectric performance and anisotropy studies of n-type Mg_3Bi_2-based single crystal. *Acta Mater.* **255**:119028. DOI:https://doi.org/10.1016/j.actamat.2023.119028.
34. Kim, S., Kim, C., Hong, Y.K. et al. (2014). Thermoelectric properties of Mn-doped Mg-Sb single crystals. *J. Mater. Chem. A* **2**(31):12311–12316.
35. Xin, J., Li, G., Auffermann, G. et al. (2018). Growth and transport properties of Mg_3X_2 (X = Sb, Bi) single crystals. *Mater. Today Phys.* **7**:61–68.
36. Ma, X., Yao, H., Zhi, S. et al. (2023). Identifying the point defects in single-crystalline Mg_3Sb_2. *Chem. Mater.* **35**:5640–5647.
37. Imasato, K., Fu, C., Pan, Y. et al. (2020). Metallic n-type Mg_3Sb_2 single crystals demonstrate the absence of ionized impurity scattering and enhanced thermoelectric performance. *Adv. Mater.* **32**:e1908218. DOI:https://doi.org/10.1002/adma.201908218.
38. Li, A., Wang, Y., Li, Y. et al. (2024). High performance magnesium-based plastic semiconductors for flexible thermoelectrics. *Nat. Commun.* **15**:5108.
39. Ma, X., Liu, K., Cao, F. et al. (2024). Single-crystalline $Mg_3Sb_{2-x}Bi_x$-based thermoelectric materials. *Cell Rep. Phys. Sci.* **5**:101875. DOI:https://doi.org/10.1016/j.xcrp.2024.101875.
40. Zhao, P., Xue, W., Zhang, Y. et al. (2024). Plasticity in single-crystalline Mg_3Bi_2 thermoelectric material. *Nature* **631**(8022):777–782.
41. Yang, J., Li, G., Zhu, H. et al. (2022). Next-generation thermoelectric cooling modules based on high-performance $Mg_3(Bi, Sb)_2$ material. *Joule* **6**:193–204.
42. Liu, Z., Gao, W., Oshima, H. et al. (2022). Maximizing the performance of n-type Mg_3Bi_2 based materials for room-temperature power generation and thermoelectric cooling. *Nat. Commun.* **13**:1120.
43. Xie, L., Yang, J., Liu, Z. et al. (2023). Highly efficient thermoelectric cooling performance of ultrafine-grained and nanoporous materials. *Mater. Today* **65**:5–13.
44. Zhou, J., Feng, J., Li, H. et al. (2023). Modulation of vacancy defects and texture for high performance n-type Bi_2Te_3 via high energy refinement. *Small* **19**:2300654. DOI:https://doi.org/10.1002/smll.202300654.
45. Zhu, W., Wei, P., Zhang, J. et al. (2022). Fabrication and excellent performances of bismuth telluride-based thermoelectric devices. *ACS Appl. Mater. Interfaces* **14**:12276–12283.
46. Zhu, Y.K., Sun, Y., Dong, X. et al. (2024). General design of high-performance and textured layered thermoelectric materials via stacking of mechanically exfoliated crystals. *Joule* **8**:2412–2424.
47. Jin, M., Lin, S., Li, W. et al. (2021). Nearly isotropic transport properties in anisotropically structured n-type single-crystalline Mg_3Sb_2. *Mater. Today Phys.* **21**:100508. DOI:https://doi.org/10.1016/j.mtphys.2021.100508.
48. Liu, J., Li, A., Fu, C. et al. (2023). Band anisotropy in thermoelectric materials. *Innov. Mater.* **1**(1):100004. DOI:https://doi.org/10.59717/j.xinn-mater.2023.100004.
49. Zhang, J., Song, L., Sist, M. et al. (2018). Chemical bonding origin of the unexpected isotropic physical properties in thermoelectric Mg_3Sb_2 and related materials. *Nat. Commun.* **9**:4716.
50. Jin, M., Liang, J., Qiu, P. et al. (2021). Investigation on low-temperature thermoelectric properties of Ag2Se polycrystal fabricated by using zone-melting method. *J. Phys. Chem. Lett.* **12**:8246–8255.
51. Lenoir, B., Cassart, M., Michenaud, J.P. et al. (1996). Transport properties of Bi-rich Bi-Sb alloys. *J. Phys. Chem. Solids* **57**:89–99.
52. Yin, L., Li, X., Bao, X. et al. (2024). CALPHAD accelerated design of advanced full-Zintl thermoelectric device. *Nat. Commun.* **15**:1468.
53. Liang, K., Yang, H., Zhao, P. et al. (2023). Characterizing the thermoelectric cooling performance across a broad temperature range. *Rev. Sci. Instrum.* **94**:105112. DOI:https://doi.org/10.1063/5.0165551.

ACKNOWLEDGMENTS

This work was supported by the Key-Area Research and Development of Guangdong Province (2024B0101040002), the Shenzhen Science and Technology Program (KQTD20200820113045081), and the GuangDong Basic and Applied Basic Research Foundation (2024B1515040022). J.M. acknowledges financial support from the National Natural Science Foundation of China (52473298), the Shenzhen Science and Technology Program (RCJC20221008092725020), the Fundamental Research Funds for the Central Universities (2024FRFK03013), the State Key Laboratory of Precision Welding & Joining of Materials and Structures (no. 24-Z-14), and the Shenzhen Stable Support Plan for Higher Education Institutions (GXWD20220818151757003). Q.Z. acknowledges financial support from the National Natural Science Foundation of China for Distinguished Young Scholars (52425108), the National Natural Science Foundation of China (52172194), and the Shenzhen Science and Technology Program (RCJC20210609103733073). F.C. acknowledges financial support from the National Natural Science Foundation of China (52472196). X.M. acknowledges financial support from the China Postdoctoral Science Foundation (2023M730841) and the National Natural Science Foundation of China (12404046).

AUTHOR CONTRIBUTIONS

J.M., Q.Z., and X.M conceived the idea; J.M. and X.M. designed the research; X.M. prepared the single crystals; X.M, S.Y., and S.Z. characterized the thermoelectric properties of single crystals; X.M. and P.Z. prepared the crystals for contact layer bonding; X.M., C.L., X.B., and J.W. prepared the thermoelectric legs with metallic contact layers; S.D., J.C., and C.L. synthesized the p-type thermoelectric materials; X.M., C.L., H.Y., K.L., and L.W. fabricated the thermoelectric coolers; C.L. and K.L. characterized and simulated the cooling performance of the device; Y.F. performed the first-principles calculation; J.M. and X.M. analyzed the data; and J.M., X.M., and Q.Z. wrote and edited the manuscript. All authors contributed helpful suggestions to this work.

DECLARATION OF INTERESTS

The authors declare no competing interests.

SUPPLEMENTAL INFORMATION

It can be found online at https://doi.org/10.1016/j.xinn.2025.100864.

LEAD CONTACT WEBSITE

http://thermoelectric.hitsz.edu.cn/
https://faculty.hitsz.edu.cn/maojun
https://faculty.hitsz.edu.cn/zhangqian